06

Multiscale structuring of CdSe/CdS/ZnS quantum dots in spin-coated and Langmuir films

© A.P. Kuzmenko,[1] E.A. Novikov,[1] M.A. Pugachevsky,[1] V.V. Rodionov,[1] V.G. Zavodinsky,[1] O.A. Gorkusha,[2] A.V. Syuy,[3] D.P. Anikin,[4] S.V. Dezhurov[5]

[1] Southwest State University, Kursk, Russia
[2] Institute of Applied Mathemativs, Khabarovsk Department, Russian Academy of Sciences, Khabarovsk, Russia
[3] Moscow Institute of Physics and Technology (National Research University), Dolgoprudny, Moscow Region, Russia
[4] RUSID,
352900 Armavir, Russia
[5] Scientific and technological testing center „Nanotech-Dubna“,
141980 Dubna, Moscow region, Russia
e-mail: apk3527@mail.ru

Received September 26, 2022
Revised April 28, 2023
Accepted May 1, 2023

A comparative analysis of the features of multiscale structuring of Langmuir and spin-coated films from stabilized TOPO (trioctylphosphine oxide) quantum dots CdSe/CdS/ZnS was carried out using optical, probe and electron microscopy methods, including high-resolution microscopy and elemental energy-dispersive analysis. The chemical structure was studied by Raman scattering, IR Fourier spectroscopy, and X-ray diffractometry. It was shown that Langmuir nanofilms built on the phenomena of self-organization are characterized by higher continuity and homogeneity, while in spin-coated films they form clusters with sizes ranging from tens to hundreds of nanometers. Calculations ab initio were performed using the electron density functional method for Cd_nSe_n nuclei, which indicated the dominance of hexagonal close packing.

Key words: micro- and nanostructuring, Langmuir-Blodgett films, spin-coated films, quantum dots, clustering.

DOI: 10.61011/TP.2023.08.57265.225-22

Introduction

The idea of creating thin films from nano-sized objects such as quantum dots (QDs) was implemented and developed for over two decades with a pronounced tendency towards an ever wider expansion of areas of practical application, for example, to opto- and nanoelectronics, sensorics [1–5]. To a significant extent, this is stimulated by the manifestation of quantum-size effects in QDs [6,7], which is due to their physical nature. QDs include mechanisms for discretizing energy levels, electron-hole pairs of the type of Bohr excitons are formed with the capabilities, in particular, of high speed response (with nonradiative electron relaxation up to $\sim 10^{-12}$ s), increasing "life time" of trap luminescence by up to three orders of magnitude. The development of the technological foundations of nanoengineering expanded the possibilities of electronic transport control in both single and multicomponent in composition and structure QDs, which made it possible to solve problems of creating optoelectronic elements with specified spectral characteristics.

In this regard, the requirements for devices and their components manufactured using QDs, as well as the compliance of the qualitative and quantitative characteristics of their structure with technological requirements, are sharply increasing. The subject of these studies was the structuring in nanofilm samples formed by spin-coating (SC) and Langmuir-Blodgett (LB) methods from semiconductor QDs CdSe/CdS/ZnS stabilized by a barrier shell of trioctylphosphine oxide (TOPO). The mechanisms of formation and structuring of nanofilms by these methods are based on the processes of self-assembly and self-organization [8–10].

1. Research target and methods

To form nanofilms, QDs with the structure „core−shell“ of the following chemical composition were used: CdSe/CdS/ZnS (Scientific and Research Institute of Applied Acoustics, Dubna). Semiconductor QDs ($A^{II}B^{VI}$), obtained by high-temperature colloidal synthesis, structurally consisted of CdSe core with a diameter of about 4 nm and two shells CdS and ZnS with a total thickness 2.5 nm. The stabilizing barrier shell was made of TOPO — $C_{24}H_{51}OP$, in contrast to [11], where amine compounds were used for this purpose. A liquid-phase colloid system (CS) with a mass concentration of QDs of 5% was created on xylene — $(CH_3)_2C_6H_4$. According to data of scanning transmission electron microscopy (STEM) [12], the thickness of the TOPO barrier shell is 0.7 nm.

In all studies, the substrates were single-crystalline silicon (100) wafers, the surfaces of which were subjected to plasma cleaning at low pressure.

The formation of a monolayer nanofilm (MNF) on aqueous subphase (de-ionized water) on a silicon substrate using the LB method was carried out on KSV Nima 2002 setup, additionally equipped with passive and active vibration protection. According to the kinetic dependences of compression isotherms — $\pi(A) = \sigma_0 - \sigma$ (π — surface pressure, A — monolayer area, σ_0 and σ — surface tensions of the subphase and monolayer) the control parameters and modes of formation of the most continuous MNFs were determined. The process of MNF formation was monitored in situ using a Brewster angle microscopy (BAM). The concentration, speed of barrier movement, substrate lifting, and temperature were varied. By changing the specified parameters the transfer coefficient [8] $k_{\text{tr}} = (S' - S'')/S_{\text{sub}}$ was brought to 1 ± 0.2. Here S' and S'' — the areas of the Langmuir monolayer at the beginning and at the end of a single transfer, S_{sub} — the area of the substrate.

The development of the spinning method made it possible to form epitaxial nanofilm structures from CS with different functional properties, in particular, piezoelectric [13]. Earlier [14] using the example of QDs from CdS stabilized by a gelatin shell using the spinning method the features of the formation of nanofilm structures by the SC method were established. spinning of the CdSe/CdS/ZnS nanofilm was carried out using a centrifuge (MiniSpin, „Eppendorf"). A droplet of CS with a volume of $0.5\,\mu$l was deposited on the substrate, which was fixed in a microtube strictly perpendicular to the axis of rotation with a radius ~ 40 mm. From a series of experiments it was established that the most continuous and homogeneous nanofilm was formed during spinning at a frequency of 4000 rpm for 10 min. To monitor the quality of MNF a confocal microscope was used, and the resulting raster images were analyzed using the original method [14].

Multiscale structuring in MNF nanofilm samples obtained by SC and LB methods was studied using microscopy methods: confocal microscopy — CM, AIST-NT OmegaScope, macro- and microscopic levels — from hundreds to tens μm), atomic force microscopy — AFM, AIST-NT SmartSPM 1000, spatial resolution by Z -coordinate — 30 pm), transmission electron microscopy — TEM, JEOL JEM -2100, accelerating voltage — 200 kV, spatial resolution —1.9Å, magnification range — from $\times 50$ to $\times 1500000$, with high resolution option — HR TEM), scanning electron (scanning electron microscopy — SEM, JEOL JSM -6610LV, accelerating voltage — up to 30 kV, spatial resolution — 3 nm, magnification range — from $\times 30$ to $\times 300000$); energy-dispersive analysis (energy-dispersive X-ray spectroscopy — EDX) using the attachment Oxford Instruments X-Max (accuracy — 0.1%); X-ray diffraction — XRD, GBC EMMA, radiation power — 2.2 kW, spot size — 12 mm, minimum goniometer step — 0.02°, goniometer radius — 180−250 mm, rotation range — 30−160°); Raman shift — RS, AIST-NT OmegaScope, radiation wavelength — 532 nm, radiation power — 50 mW, spectral resolution — 0.8 cm^{-1}, spatial resolution — $0.5\,\mu$m); IFx28xFourier-transform infrared spectroscopy — FTIR, Nicolet iS50, with measurements in the range — 50−15000 cm^{-1}, spectral resolution — 0.125 cm^{-1}).

2. Results and discussion

When analyzing the identified features of the surface morphology and the kinetics of formation of monolayer structures LB MNF [16] formed by LB method, descriptions of the ongoing processes of self-assembly and self-organization [10,15], and the conclusions of combinatorial geometry, according to which the maximum close packing of elements of the same type such as the QDs being studied should correspond to a structure with hexagonal close packing — hexagonal package (HP) [16]. The implementation of such scenario was tested by structuring MNF during the evaporation of the droplet $V = 0.5\,\mu$lon Si substrate.

The most characteristic features of multiscale ordered structuring (MOS) after evaporation of MNF droplet with CS are demonstrated by sampling CM and AFM images along the direction „center−edge" (radius 2.5 mm), presented in Fig. 1. The general appearance of the image of the evaporated droplet had radial-axial symmetry. It contained regions of so-called (according to accepted terminology, for example, [8]) pinning — at the edge; stagnation — in the region with a thin-film structure, depleted with QDs and filled with transparent crystallites of xylene and TOPO; center — with cluster structures. Fragments of these regions are illustrated with multiscale magnification (from macro- to nano-level). The occurrence of concentric bands with sizes from 10 to $200\,\mu$m (bottom row of CM images in Fig. 1) was noted. In the top row in Fig. 1 there are CM images with magnification up to $\times 2830$, obtained using optical zoom. Cluster structures made of QDs with dimensions ~ 100 nm are also shown here (AFM images in the top row in Fig. 1). In the stagnation region a typical interference pattern on a thin film was observed.

Based on the results of granulometric analysis of the height distribution from AFM images presented in Fig. 1 a difference of an order of magnitude in the sizes of the constituent structures was established. Thus, the structures forming the nodes had dimensions $d_{av\ n} \sim 100$ nm (left AFM image, Fig. 1), while the sizes of nanoclusters of QDs filling the stagnation region (right AFM image, Fig. 1) — $d_{av\ st} \sim 10$ nm. The order of sequence of colors in the interference pattern in CM images in the stagnation region corresponds to changes in the thickness of the wedge-shaped film structure due to the redistribution of the sizes of nanoclusters of QDs. This is consistent with the conclusions and descriptions presented in [8,17] during free evaporation of CS droplet, as well as after spinning [14,15] or electrical impact on nano-sized systems [18], which are natural for the processes of self-assembly and self-organization.

For comparison, Fig. 2 summarizes the most typical AFM, TEM images, including HR TEM, SEM with EDX, illustrating the MOS features during the formation of

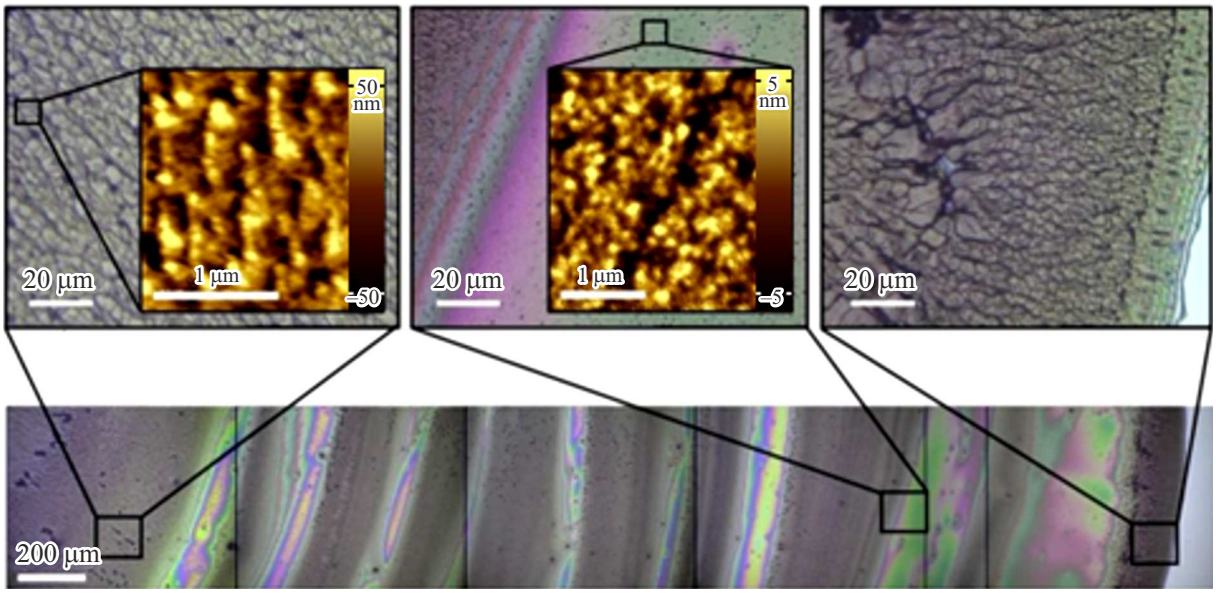

Figure 1. A series of typical confocal and atomic force images of multiscale structuring of film during the free evaporation of droplet from TOPO-stabilized QDs CdSe/CdS/ZnS.

CdSe/CdS/ZnS type CS nanofilms on silicon substrates by LB and SC methods.

Fig. 2, *a* with inserts *1*–*5* illustrates MOS nanofilms obtained by the SC method. Inserts *1*and *2* show typical AFM images of nanofilm with scales 150 × 150 nm and 1 × 1 μm, respectively, which indicated MOS ordering at the nanoscale level. The lateral sizes of spherical clusters — up to 100 nm (inset *1*). As can be seen from a more detailed AFM image (inset *2*), they are represented by nanoclusters, the lateral dimensions of which did not exceed 30 nm, their height coincided with the dimensions of QDs, amounting to about 4 nm [11]. Note that previously [14], based on data of small-angle X-ray scattering, two maxima were identified in the lateral size distribution of nanoparticles in such a nanofilm, approximately 5 and 20 nm. Good agreement between these sizes and their values in AFM images can serve as an argument in favor of local both multilayer and monolayer nature of such nanofilm structures. This conclusion is further supported by inserts *3* and *4* with TEM images with a resolution of 50 nm and their view in HR TEM mode with resolution of 20 nm, respectively. Moreover, the electron diffraction pattern (insert *5*) had a characteristic amorphous halo and some diffraction reflections (from the substrate), which also confirmed this assumption. This is in good agreement with the results [13].

In a simplified form, the equation of motion presented in [14], for each QD with mass m_i at some position relative to the axis of rotation — r_i in a rectangular coordinate system limits the action of forces in the plane of the rotating substrate only by viscous friction and centrifugal force: $m_i d^2 r_i/dt^2 = 4\pi^2 \nu^2 m_i r_i - (\eta S_i/h)\, dr_i/dt$. Here ν — centrifuge rotation speed, η — dynamic viscosity of the solution, S_i — substrate area under the QD, h — particle position along the layer height in CS. The solution to this equation is the expression: $r_i = r_{i0} \exp(-kt/h) \operatorname{ch}(2\pi\nu t)$, in which r_{i0} — the initial position of the QD, k — the dimensional constant determined by the viscosity and surface area of the particle. Of interest is the minimum height of the CS layer, which is obviously limited by the diameter of the particle, and actually corresponds to the monolayer formation of nanofilms by the spinning method, when, under conditions of mutual compensation of friction and centrifugal forces, the dominant effect on the particle is the adhesive bond force. These considerations did not take into account the Van der Waals interaction, by which clustering can occur with the formation of the actually observed MOS (Fig. 1, 2, *a*).

Fig. 2, *b* (with inserts *1*–*9*) presents data of microscopic (AFM, SEM, TEM, HR TEM) and elemental analysis (SEM EDX) of MOS in LB films. Previously, it was shown that phase transitions along the $\pi(A)$ isotherm during the formation of LB monolayer were accompanied by the transformation of tetragonal close packing into hexagonal one, which was consistent with the conclusions based on combinatorial geometry. In the insert *1* with AFM image (in the fregion with dimensions 100 × 100 nm), the fragments were selected with structures isomorphic to the cubic, triclinic and hexagonal systems, which are formed from nanoclusters (designation with the corresponding with schematic callouts: Triangular-like, Square-like, Hexagonal-like). Note that this approach was used to analyze the structuring of films made of metal-containing organic compounds [16]. Triangular-like image, which is callout from the main AFM image, shows a line along which a height profile was plotted using the Gimp graphic editor (insert *2*). The length of the marked line obtained in this

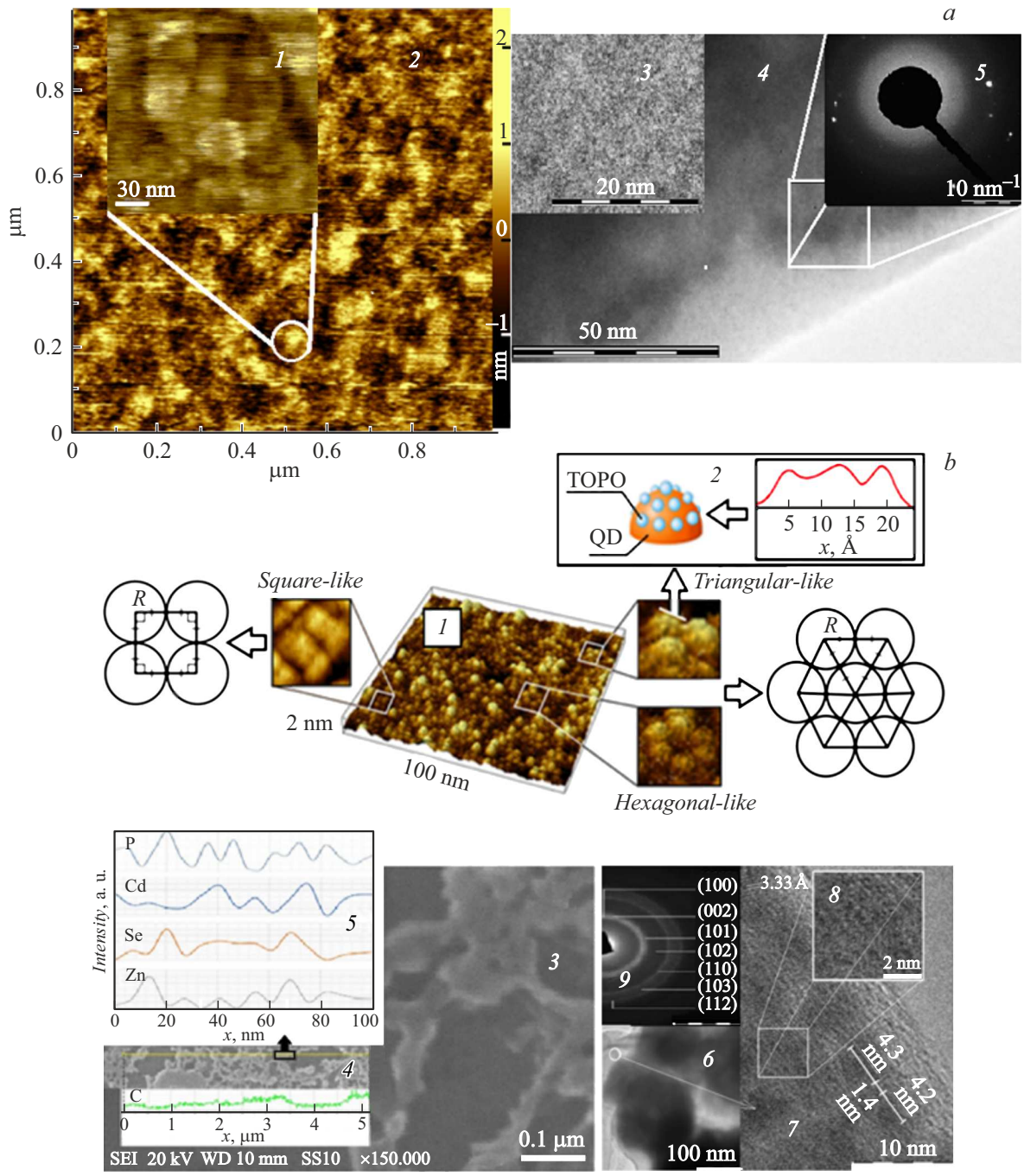

Figure 2. Microscopic images of multiscale ordered structuring of MNF of QDs CdSe/CdS/ZnS stabilized by TOPO method: *a* — spinning; *b* — LB. All digital designations are described in the text.

way was 25 Å, and the profile of intensity changes along it had a periodic nature with a step of 0.5 nm, which is consistent with the thickness of the shell (one TOPO molecule) according to the results of STEM [12].

The insert *3* of Fig. 2, *b* shows SEM image of the surface of single-layer LB nanofilm in a specially selected region with obvious discontinuities. EDX analysis was carried out on this section 5 μm long (insert *4*). Carbon concentration distribution profile in TOPO — $C_{24}H_{51}OP$ is also shown here. Against a generally uniform background of C concentration, its increase by almost 2 times is noticeable in regions with nanofilm. In a section 100 nm long in the nanofilm marked in the insert *4*, the concentration distributions of the elements Zn, Se, Cd and P, components of the QDs, were obtained, which turned out to be close to periodic (insert *5*). Thus, for changes in P concentration this period was 13 nm. Relating magnitude it was consistent with the data on sulfur in CdS and ZnS compounds obtained by the STEM method [19].

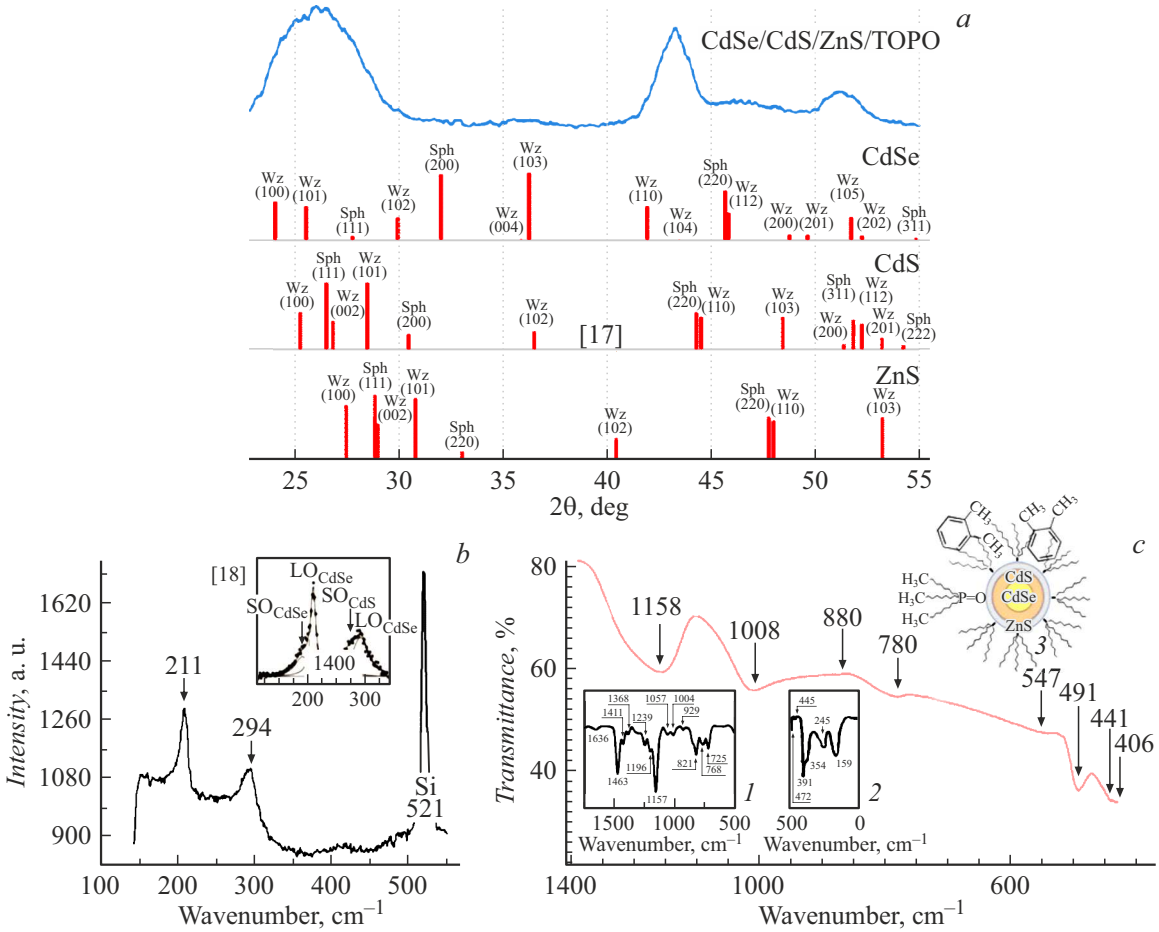

Figure 3. Structure of LB nanofilms according to analysis data: X-ray diffraction with lines from the ISSD database [21] (*a*), Raman (*b*) with an insert from [22] and Fourier IR (*c*). Shown in the insets: *1* — for TOPO from [23], *2* — for xylene from [24], *3* — schematic representation of QDs with TOPO shell in xylene based colloidal system.

According to our data obtained using TEM (inserts *6* and *7* in Fig. 2, *b*), in LB films (in contrast to spin-coated films — insert *5* in Fig. 2, *a*) the formation of MOS had a crystalline ordering (insert *9*), which was fully consistent with [20]. The following series of atomic planes was discovered for wurtzite and sphalerite: (100), (002), (101), (102), (110), (103) and (112). In the insert *7* in the HR TEM mode the regions with electron diffraction on gratings in two neighboring CdSe nuclei with a size of 4 nm are highlighted, which is completely consistent with the manufacturer's datasheet and the results for QDs without TOPO [{]11 }. As noted above, the hydrodynamic size of an individual QD with TOPO [14], as measured by small-angle X-ray scattering (SAXS), was 5 nm, i.e. included 2 semiconductor (CdS and ZnS) shells, but without taking into account the contribution of the barrier shell due to the small atomic masses of the chemical elements in its composition. Assuming that there is no mutual penetration of barrier shells of adjacent QDs, the thickness of one TOPO shell was determined from the TEM image (insert *7*) to be 0.7 nm, which exactly coincided with its value in [12]. The characteristic lattice period 0.333 nm is also shown here. The overlap of several crystal lattices due to minor disturbances in monolayering was noted, which led to the formation of diffraction characteristic of binary lattices, as illustrated by the insert *8*.

The results of XRD, RS and FTIR analyzes of MNF samples obtained by the LB method are shown in Fig. 3. The crystal structure, determined by XRD and shown in Fig. 3, *a*, was measured in standard Bragg-Brentano geometry at the CuK_α line. The diffraction pattern contained three very broad reflections with maximum intensity at angles $2\Theta = 25$, 42 and 50 °. Such a significant expansion of the reflections is due to both the superposition of lines for planes (100), (110), (103), corresponding to the cubic system of each of the compounds CdSe, CdS, ZnS, and the sizes of QDs nanoparticles in the composition of MNF and MOS, which also noted in [25,26]. To illustrate the additive contribution to the resulting diffraction pattern of the crystal structures of wurtzite and sphalerite, their characteristic lines (with angles and intensities) are given in accordance with the ISSD base [21]. This conclusion is consistent with the results in [5,12], where the separation of contributions from each of the compounds in the

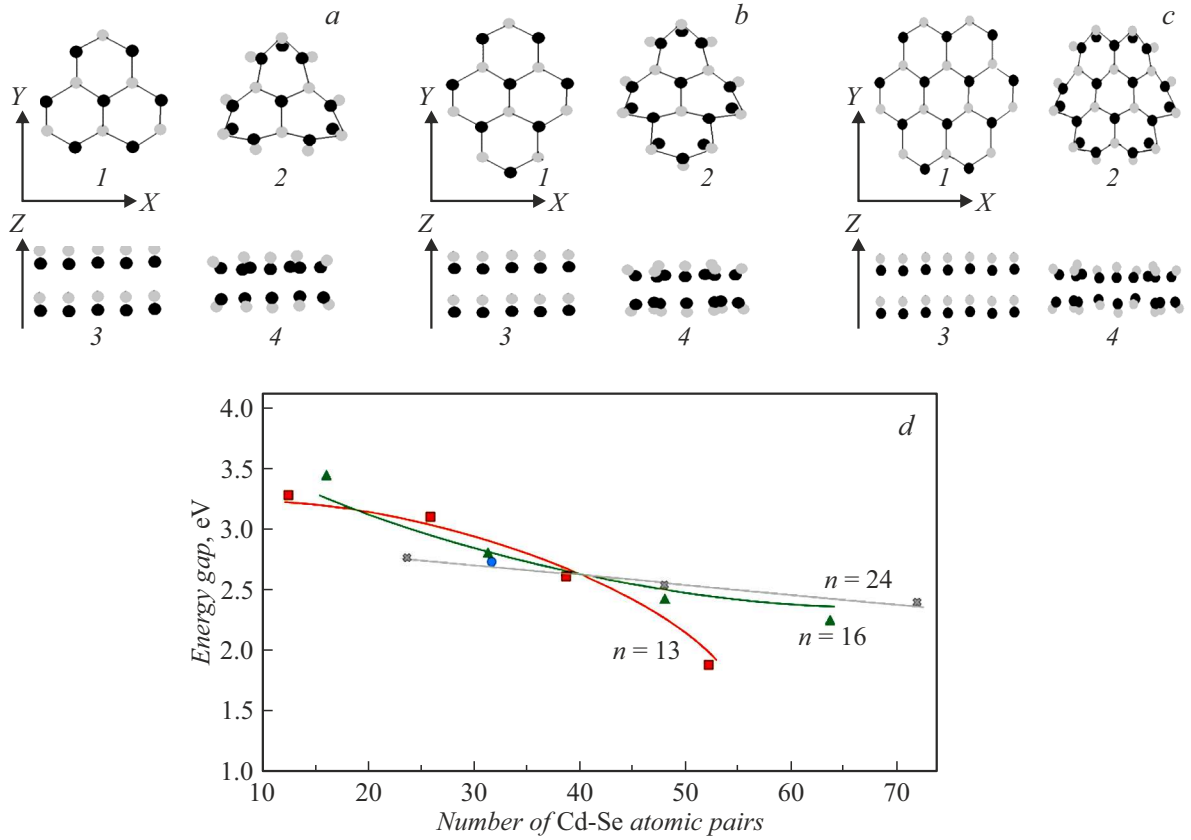

Figure 4. Initial formulation ($a-c$) and modeling results (d): „wurtzite“ structures (“top“ view — in the plane XY — *1, 2*; “side“ view — along the axis Z — *3, 4* particlesCd_nSe_n (black circles — Cd, gray — Se) for: $a - n = 13-Cd_{13}Se_{13}$, $b - n = 16-Cd_{16}Se_{16}$, $c-n = 24-Cd_{24}Se_{24}$. *1, 3* — starting configurations, *2, 4* — after relaxation; changes E_b (n) — *d*.

QDs composition was noted with increase in thickness of the barrier shell to values significantly exceeding 0.7 nm. The coherent scattering region estimated from the Debye-Scherrer-Selikhov formula was 3.5 nm, i.e. was consistent with the measured dimensions of the QDs using SAXS [10].

The chemical structure of MNF deposited on a substrate with surface enhancement effect (SERS) was studied by the RS method (Fig. 3, *b*). Excitations in the silicon substrate with SERS produced the most intense line — 521 cm^{-1} and confirmed the reliability of the obtained spectrum. For the CdSe core the RS spectrum contained characteristic optical modes: longitudinal (LO_{CdSe} — 211 cm^{-1} with the second harmonic 422 cm^{-1}) and a very weak surface (SO_{CdSe} — 187 cm^{-1}), consistent with [27,28]. A wide band in the vicinity of 294 cm^{-1} arose due to confinement on optical phonons on the CdSe core and in the thin shell of CdS — LOCdS and SOCdS, which was consistent with the conclusions [22]. A more detailed analysis of the RS spectra of CdSe/CdS QDs with shell of 3 nm (our shell — 0.7 nm) [12] revealed an increase in intensity by several times in the region of 294 cm^{-1} due to excitation LO_{CdS} — 294 and SO_{CdS} — 267 cm^{-1}. It is also shown here that at the boundary „core–shell“ compounds arise with lines 199 and 284 cm^{-1}. The lognormal shape of the intensity change in this region (Fig.. 3, *b*) is due to the additive contribution of thin shells of both CdS and ZnS, which is consistent with the lines LO_{CdS}: — 290 [28] and LO_{ZnS} — 310 cm^{-1} [27].

The FTIR spectrum of the colloidal system, including CdSe/CdS/ZnS QDs, with stabilizing TOPO shell, in xylene solution in the region less than 1400 cm^{-1} was studied (Fig. 3, *c*). In the indicated range, it is represented predominantly by deformation vibrations ν(P–C) from 1008 to 1158 cm^{-1} and ν(P=O): 780 and 880 cm^{-1} according to the chemical formula TOPO $-C_{24}H_{51}OP$. Lines 406, 441, 491, 547 cm^{-1} corresponded to xylene impurity inclusions — $(CH_3)_2C_6N_4$. These conclusions are confirmed by the FTIR spectrum for the TOPO barrier shell [23]. Here, in the insert *2*, there is a fragment of the FTIR spectrum for ortho-xylene from [24]. In the insert *3* the original TOPO shell is supplemented with inclusions of sorbed xylene, which is retained due to hydrophobic interaction with octyl radicals in the TOPO composition. It is possible that the presence of these inclusions caused discontinuities in the LB films (Fig. 2).

The commonality of the crystal structures of all CdSe, CdS, and ZnS compounds included in QDs allows us to carry out model calculations for the two most characteristic stable structures: hexagonal wurtzite (*w*-CdSe) and cubic

sphalerite (*s*-CdSe). Using the example of *w*-CdSe, in accordance with density functional theory [29] in FHI96md [30] software package based on pseudopotentials from package FHI98pp [31], test calculations were carried out. Fig. 4, *a*–*c* schematically shows the initial and final structures that arise under the action of volumetric compression. The effect of compression on CdSe particles was previously confirmed by XRD data [32] and changes in the RS spectrum [28] when the formation of alloys CdS_{al} , $CdSe_{al}$ + CdS_{al}, and $CdSe_{al}$. Under our conditions, it may be due to the influence on the CdSe core of both two semiconductor shells CdS, ZnS, and TOPO with xylene, especially after they dry.

According to Fig. 4, *a*–*c*, calculations were carried out for three types of changes *n* from the initial state with the corresponding number of Cd and Se atoms ($n = 13$, 16 and 24) for the hexagonal structure of Cd and Se (columns with odd numbers — 1 and 3 and columns with even numbers — 2 and 4) with a multiple increase in their number according to the arithmetic progression $n = n(k + 1)$, where $k = 0$, 1, 2, 3. The Figure shows all the characteristic movements of external Cd atoms between Se layers with decreasing interatomic distances, which is consistent with the results of XRD [32] and RS [28] for CdSe nanoparticles.

Fig. 4, *d* shows the calculated values of the band gap $E_g(n)$ for three modifications of the structure in CdSe with a multiple increase in the number of forming Cd and Se atoms. With an increase in particle size from 0.5 to 1.2 nm, a decrease in the calculated E_g from 3.3 to 2.2 eV was noted. When extrapolating the number of pairs Cd–Se to 130 particles, they increased in size to 2 nm and acquired a predominant structure of the "wurtzite"type — *w*-CdSe.

The presence in the AFM image (Fig. 2, *b*) of structures of Triangular-like, Square-like and Hexagonal-like types on the corresponding callouts confirms this conclusion. The specific area on the MNF surface of each QD — *A*, determined from the isotherm $\pi(A)$, was the sum of its own area and two adjacent hypocycloid Triangular-like slits. For HP packaging this value was $A_6 = 2R^2(3)^{1/2}$. Whereas in tetragonal package (TP) its value is equal to $A_4 = 4R^2$. Thus, A_6 is less (which is energetically more favorable) than A_4. When depositing films from QD by the LB method, the transition from the „liquid-phase„ MNF state with TP ordering (as it approaches collapse on the isotherm $\pi(A)$) to „solid-phase" state, accompanied by a hexagonal-like — from *w*-CdSe.

Raman shifts (Fig. 3, *b*), partial amorphous halo in the crystal structure of QDs (Fig. 2, *b*, insert *9*), periodicity in distributions P, Cd, Se, Zn (Fig. 2, *b*, insert *5*), also as the QD sizes according to HR TEM data (minimum 4 nm, Fig. 2, *b*, insert *7*) confirmed the validity of the calculations of the values $E_b(n)$ specifically for the wurtzite structure (Fig. 4, *d*), which is consistent with the conclusions on the minimum energy for *w*-CdSe crystals — first-order phase transition „liquid–solid" and their HP ordering.

Conclusion

A comparative analysis of the multiscale structuring of nanofilms of CdSe/CdS/ZnS quantum dots stabilized by TOPO in colloidal system of xylene solution, formed by spinning and LB methods, was carried out. It is shown that at the phenomena of self-assembly and self-organization combining both methods the nanofilms deposited by the Langmuir method have higher continuity and planar uniformity of the distribution of quantum dots over the surface of the substrate. It is established that monolayer formation of nanofilms from quantum dots by spinning is achieved only in narrow localized areas under conditions of mutual compensation of friction and centrifugal forces, when the action of the adhesive bond force becomes dominant. The formed structures are characterized by amorphism and are represented by clusters with sizes ranging from tens to hundreds of nanometers; the mechanism of their multiscale structuring is based on self-organization phenomena. It is shown that the formation of Langmuir nanofilms obeys the logic of combinatorial geometry with a pronounced tendency for ordering in the form of the most close hexagonal packing of nanoclusters of quantum dots with a predominantly wurtzite structure on the substrate. This conclusion is confirmed by model calculations performed on the basis of density functional theory using the example of the compound Cd_nSe_n, which constitutes the core of quantum dots, for which, with the number of atomic pairs Cd–Se equal to 130, extrapolation of the calculated energy value E_g corresponds to a size of 2 nm, which is consistent with the obtained empirical data.

Acknowledgments

The authors thank the staff of the D.V. Krylsky, employee of Scientific and Research Institute of Applied Acoustics (Dubna) for providing a sample of CdSe/CdS/ZnS quantum dots stabilized by TOPO.

Funding

The study was carried out with financial support from the Ministry of Education and Science of the Russian Federation (s/o 2020 № 0851-2020-0035) within the framework of the implementation of the strategic academic leadership program „Priority-2030" (Agreement № 075-15-2021- 1213).

Conflict of interest

The authors declare that they have no conflict of interest.

References

[1] C.J. Murphy, J.L. Coffer. Appl. Spectrosc., **56**, 16A (2002).
[2] H. Kudilatt, B. Hou, M.E. Welland. Part. & Part. Syst. Charact., **37**, 2000192 (2020). DOI: 10.1002/ppsc.202000192

[3] K. Khan, A.K. Tareen, M. Aslam, R. Wang, Y. Zhang, A. Mahmood, Z. Ouyang, H. Zhang, Z. Guo. J. Mater. Chem, **8**, 387 (2020). DOI: 10.1039/C9TC04187G
[4] R. Ma, Z. Tian, Y. Hu, Y. Huang, J. Lu. Langmuir, **34**, 11354 (2018). DOI: 10.1021/acs.langmuir.8b02232
[5] K.-P. Chang, Y.-C. Yeh, C.-J. Wu, C.-C. Yen, D.-S. Wuu. Nanomaterials, **12**, 909 (2022). DOI: 10.3390/nano12060909
[6] S.A. Sergeev, M.V. Gavrikov, N.D. Zhukov. Pis'ma v ZhTF, **48**, 32 (in Russian). (2022). DOI: 10.21883/PJTF.2022.09.52448.19115
[7] E. Petryayeva, W.R. Algar, I.L. Medintz. Appl. Spectrosc., **67**, 215 (2013). DOI: 10.1366/12-06948
[8] L.V. Andreeva, A.V. Koshkin, P.V. Lebedev-Stepanov, A.N. Petrov, M.V. Alfimov. Coll. Surf., A: Physicochem., Eng. Aspects, **300**, 300 (2007). DOI: 10.1016/j.colsurfa.2007.02.001
[9] B. Martín-García, M.M. Velazquez. Langmuir, **30**, 509 (2014). DOI: 10.1021/la404834b
[10] A.P. Kuzmenko, E.A. Novikov, V.V. Rodionov, A.V. Kuzko, D.P. Anikin, D.V. Krylsky. Izvestiya YuZGU.. Seriya: Tekhnika i tekhnologii, **2**, 86 (2021). (in Russian).
[11] A.G. Vitukhnovsky, A.A. Vashchenko, D.N. Bychkovsky, D.N. Dirin, P.N. Tananaev, M.S. Vakshtein, D.A. Korzhonov. FTP, **47**, 1591 (2013). (in Russian).
[12] J. Xu, X. Ji, K.M. Gattas-Asfura, C. Wang, R.M. Leblanc, Coll. Surf., A: Physicochem., Eng. Aspects, **284**, 35 (2006). DOI: 10.1016/j.colsurfa.2005.11.046
[13] M.V. Kelso, N.K. Mahenderkar, Q. Chen, J.Z. Tubbesing, J.A. Switzer. Science, **364**, 6436 (2019). DOI: 10.1126/science.aaw6184
[14] A.P. Kuzmenko, E.A. Novikov, M.A. Pugachevsky, V.M. Emelyanov, O.I. Shutyaeva. Izvestiya YuZGU.. Seriya: Tekhnika i tekhnologii, **3**, 88 (2019). (in Russian).
[15] K.A. Svit, K.S. Zhuravlev. Semiconductors, **53**, 1540 (2019). DOI: 0.1134/S1063782619110198
[16] P. Alexandridis, U. Olsson, B. Lindman. Langmuir, **14**, 2627 (1998). DOI: 10.1021/la971117c
[17] A.P. Kuzmenko, Ch.N. Aung, V.V. Rodionov. ZhTF, **6**, 118 (2015) (in Russian).
[18] A.P. Kuz'menko, T.P. Naing, A.E. Kuz'ko, M.M. Tan. Tech. Phys., **65** (2), 254 (2020). DOI: 10.1134/S1063784220020127
[19] P. Adel, A. Wolf, T. Kodanek, D. Dorfs. Chem. Mater., **26**, 3121 (2014). DOI: 10.1021/cm500431m
[20] J. van Embden, J. Jasieniak, P. Mulvaney. ASC, **131**, 14299 (2009). DOI: 10.1021/ja9030209
[21] Powder Diffraction File, Joint Committee on Powder Diffraction Standards, ASTM, Philadelphia, PA, 1967, Card 2−549, Card 19−191
[22] L.B. Hai, N.X. Nghia, P.T. Nga, V.D. Chinh, N.T.T. Trang, V.T.H. Hanh. J. Exp. Nano., **4**, 277 (2009). DOI: 10.1080/17458080802178619
[23] R. Liu, Y. Geng, Z. Tian, N. Wang, M. Wang, G. Zhang, Y. Yang. Hydrometallurgy, **199**, 105521 (2021). DOI: 10.1016/j.hydromet.2020.105521
[24] T. Prabhua, S. Periandy, S. Ramalingama. Spectrochim. Acta Part A, **79**, 948 (2011). DOI: 10.1016/j.saa.2011.04.001
[25] X. Wang, W. Li, K. Sun. J. Mater. Chem., **21** (24), 8558 (2011). DOI: 10.1039/c1jm00061f
[26] R.K. Ratnesh, M.S. Mehata. Opt. Mater., **64**, 250 (2017). DOI: 10.1016/j.optmat.2016.11.043
[27] D.K. Guptaa, M. Verma, K.B. Sharma, N.S. Saxena. Indian J. Pure & App. Phys., **55**, 113 (2017). DOI: 10.56042/ijpap.v55i2.14671
[28] M.V. Dzhagan, M.Ya. Valakh, A.G. Milekhin, N.A. Yeryukov, R.T.D. Zahn, E. Cassette, Th. Pons, B. Dubertret. J. Phys. Chem. C, **117**, 18225 (2013). DOI: 10.1021/jp4046808
[29] W. Kohn, J.L. Sham. Phys. Rev., **140**, A1133 (1965).
[30] M. Beckstedte, A. Kley, J. Neugebauer, M. Scheffler. Comp. Phys. Comm., **107**, 187 (1997).
[31] M. Fuchs, M. Scheffler, Comp. Phys. Comm., **119**, 67 (1999). DOI: 10.1016/S0010-4655(98)00201-X
[32] S. Neeleshwar, C.L. Chen, C.B. Tsai, Y.Y. Chen, C.C. Chen, S.G. Shyu, M.S. Seehra. Phys. Rev. B: Condens. Matter Mater. Phys., **71**, 201307 (2005). DOI: 10.1103/PhysRevB.71.201307

Translated by I.Mazurov